Inorganic Chemistry

Communication

Cite This: Inorg. Chem. 2019, 58, 52−56

pubs.acs.org/IC

Tetrathiafulvalene-Based Helicene Ligand in the Design of a Dysprosium Field-Induced Single-Molecule Magnet

Fabrice Pointillart,*[,†] Jiang-Kun Ou-Yang,[†] Guglielmo Fernandez Garcia,[†,‡] Vincent Montigaud,[†] Jessica Flores Gonzalez,[†] Rémi Marchal,[†] Ludovic Favereau,[†] Federico Totti,[‡] Jeanne Crassous,*[,†] Olivier Cador,[†] Lahcène Ouahab,[†] and Boris Le Guennic*[,†]

[†]Univ Rennes, CNRS, ISCR (Institut des Sciences Chimiques de Rennes) - UMR 6226, 35000 Rennes, France

[‡]Department of Chemistry "Ugo Schiff" and INSTM RU, University of Florence, 50019 Sesto Fiorentino, Italy

Supporting Information

ABSTRACT: The design of a coordination complex that involves a ligand combining both a tetrathiafulvalene core and a helicene fragment was achieved thanks to the reaction between the new 2-{1-[2-methyl[6]helicene]-4,5-[4,5-bis(propylthio)tetrathiafulvalenyl]-1*H*-benzimidazol-2-yl}pyridine ligand (**L**) and the $Dy(hfac)_3{\cdot}2H_2O$ metalloprecursor. Magnetic investigations showed field-induced single-molecule-magnet (SMM) behavior under an applied magnetic field of 1000 Oe for $[Dy(hfac)_3(\mathbf{L})]{\cdot}0.5CH_2Cl_2$, while experimentally oriented single-crystal magnetic measurements allowed for determination of the magnetic anisotropy orientation. The magnetic behavior was rationalized through ab initio CASSCF/SI-SO calculations. This redox-active chiral-field-induced SMM paves the way for the design of switchable-multiproperty SMMs.

Chemists are working hand in hand with physicists to design single-molecule magnets (SMMs) displaying magnetic bistability at temperatures as high as possible. Recently, a mononuclear Dy^{III}-SMM highlighted a blocking temperature of 60 K,[1−3] jump-starting the kind of molecular objects suitable for potential applications in high-density data storage, quantum computing, and spintronics.[4−6] One more challenge is to combine the SMM behavior with other chemical, optical, or physical properties such as ferroelectricity, redox activity/conductivity, luminescence, nonlinear optics, and chirality/chiroptical activity in order to open the way for more potential applications.[7−9] In the specific case of chiral SMMs, the chirality can come from highly optically active ligands such as [*n*]helicenes,[10,11] which are organic molecules with a π-conjugated helical backbone made of ortho-fused aromatic rings with configurational stability for $n \geq 5$.[12] Subsequently, the [*n*]helicenes can be decorated by an electroactive unit such as organometallic,[13] quinone,[14] pyridinium,[15] and tetrathiafulvalene (TTF)[16] derivatives. The latter TTF core is a well-known electroactive fragment mainly used to design conducting materials ranging from semiconductors to superconductors.[17,18] Its functionalization with a plethora of accepting groups allowed the TTF-based ligands to participate in the development of fluorescence switches,[19] photovoltaic cells,[20] coordination of transition metals,[21] and finally coordination of 4f elements. In particular, the combination of lanthanide ions with TTF-based ligands permitted one to reach new classes of multiproperty compounds with redox-active luminescent SMM behavior.[7,22] To the best of our knowledge, no chiral SMM with a redox activity easily chemically accessible in common organic solvents has been reported to date. To reach such an objective, we propose (i) to combine both electroactive TTF and carbo[6]helicene in a unique ligand and (ii) to coordinate such a ligand to a magnetically anisotropic Dy^{III} ion.

Functionalization of the molecular skeleton 4,5-bis(propylthio)tetrathiafulvalenyl]-1*H*-benzimidazol-2-yl}-pyridine[23] with 2-bromomethyl[6]helicene[24] in its racemic form (85% yield; see the Supporting Information, SI) led to the 2-{1-[2-methyl[6]helicene]-4,5-[4,5-bis(propylthio)-tetrathiafulvalenyl]-1*H*-benzimidazol-2-yl}pyridine (**L**) ligand, which reacted with the precursor $Dy(hfac)_3{\cdot}2H_2O$ ($hfac^-$ = 1,1,1,5,5,5-hexafluoroacetylacetonate anion) to give the mononuclear complex $[Dy(hfac)_3(\mathbf{L})]{\cdot}0.5CH_2Cl_2$.

Single-crystal X-ray diffraction confirms that this compound crystallizes in the triclinic space group $P\bar{1}$ (No. 2; Table S1). The molecular structure attests to the success of alkylation of the TTF-based molecular skeleton by the 2-methylenecarbo[6]-helicene derivative (Figures 1 and S1). The Dy^{III} ion is coordinated to the bischelating 1*H*-benzimidazol-2-yl}pyridine (bzip) moiety and to the three $hfac^-$ anions in a surrounding N_2O_6. From a strict structural point of view, the first neighboring atoms create a D_{2d} symmetry polyhedron (Table S2; *SHAPE* analysis[25]). The neutrality of ligand **L** is confirmed by the C9═C10 central bond length of 1.343(7) Å. The benzimidazole−TTF fragment is planar, while the planes formed by the benzimidazole and pyridine moieties have a twist angle of 18.0(2)°, resulting from the steric hindrance of the [6]helicene arm and optimized π−π interactions between the terminal benzene ring of the helicene and the bzip-coordinated fragment. A quick overview of the literature on these kinds of TTF-based ligands shows a zero twist angle when no alkylation is realized (amine, NH)[26] and for methyl-2-pyridine,[27] 4-methylpyridine-*N*-oxide,[27] and 4,4′-dimethyl-2,2′-bipyridine[28] as alkylating arms, while a twist angle of 12.2(3)° is measured for a bulkier arm such as 2,6-di(pyrazol-1-yl)-4-methylpyridyl.[29] The crystal packing highlights the formation of a one-dimensional network

Received: October 5, 2018
Published: December 14, 2018

DOI: 10.1021/acs.inorgchem.8b02830
Inorg. Chem. 2019, 58, 52−56

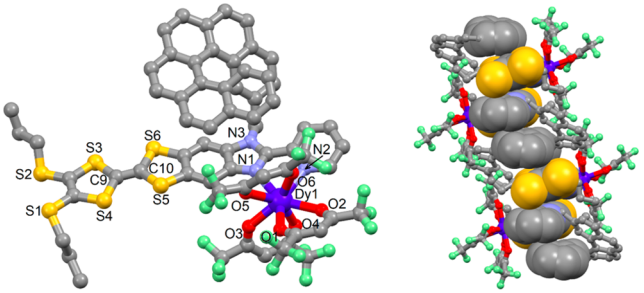

Figure 1. (Left) Molecular structure of $[Dy(hfac)_3(\mathbf{L})]\cdot 0.5CH_2Cl_2$. The hydrogen atoms and dichloromethane molecule of crystallization were omitted for clarity. Selected bond lengths (Å): Dy1−N1, 2.466(5); Dy1−N2, 2.562(5); Dy1−O1, 2.330(4); Dy1−O2, 2.366(4); Dy1−O3, 2.332(4); Dy1−O4, 2.351(4); Dy1−O5, 2.372(4); Dy1−O6, 2.323(4); C9−C10, 1.343(7); carbon (C, gray); fluorine (F, green). (Right) Crystal packing of $[Dy(hfac)_3(\mathbf{L})]$ highlighting the $\pi-\pi$ interactions along the *a* axis between the TTF-based molecular skeletons and the helicenic moieties (spacefill representation).

of stacked **L** along the *a* axis, which is formed by intramolecular $\pi-\pi$ interactions between the helicene and bzip fragments and intermolecular $\pi-\pi$ interactions between two "head-to-tail" ligands (Figure 1). The shortest intermolecular Dy−Dy distance is equal to 9.529 Å.

The redox properties of ligand **L** and complex $[Dy(hfac)_3(\mathbf{L})]\cdot 0.5CH_2Cl_2$ are investigated by cyclic voltammetry (Figure S2 and Table S3). The cyclic voltammogram for the free ligand shows two monoelectronic oxidations at 0.53 V for the first oxidation and 0.93 V for the second oxidation, corresponding to the formation of a radical cation and a dication TTF fragment, respectively.[23,26−29] Coordination of the $Dy(hfac)_3$ fragment has almost no significant effect on the oxidation potentials (0.55 and 0.94 V), as observed for similar compounds.[26−29] The electrochemical properties attest to the fact that the reversibility of the oxidation potentials and redox activity of the ligand are conserved after complexation.

The temperature dependence of $\chi_M T$ for a powdered sample of $[Dy(hfac)_3(\mathbf{L})]\cdot 0.5CH_2Cl_2$ shows a room temperature value of 14.06 cm^3 K mol^{-1} in agreement with an isolated Dy^{III} ion (Figure 2a). Upon cooling, $\chi_M T$ decreases monotonically to 12.17 cm^3 K mol^{-1} at 2 K. The first magnetization at 2 K highlights a classic behavior in the field range of 0−50 kOe for such an isolated Dy^{III} ion (inset in Figure 2a). The same sample shows a frequency dependence in zero external direct-current (dc) field (Figures 2b and S3) but with a maximum of the χ_M'' versus ν curve [ν is the frequency of the alternating-current (ac) oscillating field] that falls out of the frequency range of the experimental window. The application of an external dc field cancels the quantum tunneling of magnetization (QTM), and the maximum of the χ_M'' versus ν curve shifts to lower frequency (Figure 2b). The 1000 Oe value was chosen as the optimum field because the relaxation is the slowest and most intense (Figure 2b). In such an applied field, both in-phase and out-of-phase components of χ_M were observed in the temperature range of 2−8 K (Figures 2c and S4). The frequency dependence of the ac susceptibility can be analyzed in the framework of the extended Debye model both for field and temperature variations. The temperature dependence of the relaxation time at 1000 Oe is extracted from the extended Debye model between 2.0 and 6.0 K (Table S4). The Arrhenius plot of the relaxation time is well fitted by a Raman relaxation process $\tau = CT^n$ with $C = 2.4(4) \times 10^{-2}$ and $n = 5.5(1)$ (Figure 2d).[29] Theoretically, the expected value of the *n* exponent for Kramers ions is 9 and can be decreased down to 4, depending on the energies of the ground-state doublets.[30,31] Recently, it is was shown that such an exponent could reach a value close to 2 because of the presence of both acoustic and optic phonons in specific ligand environments.[32] The Cole−Cole[33] plots normalized to their isothermal value are represented in Figure S5. The Dy^{III} ion lies in a N_2O_6 environment with the two nitrogen atoms coming from a bischelating imidazol-2-ylpyridine derivative, while the six oxygen atoms come from three $hfac^-$ anions. Thus, the extracted dynamic parameters for complex $[Dy(hfac)_3(\mathbf{L})]\cdot 0.5CH_2Cl_2$ can be compared with examples in which the common TTF-based skeleton is alkylated with different chemical arms.

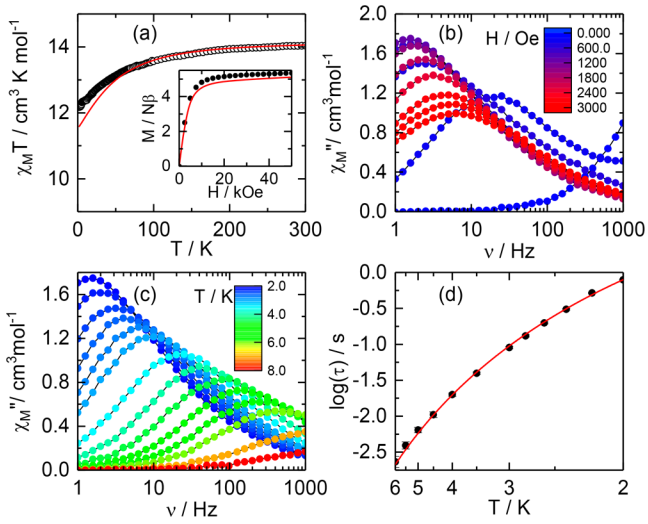

Figure 2. (a) Thermal variation of $\chi_M T$. Inset: First magnetization. Calculated curves are in red. (b) Scan field of the frequency dependence of χ_M'' at 2 K. (c) Frequency dependence of χ_M'' between 2 and 8 K at 1000 Oe. (d) Temperature variation of the relaxation time measured in an external field of 1000 Oe with the best-fitted curve (red line) in the temperature range of 2−6 K.

In these compounds and others of the literature,[34] the effective energy barrier ranges from 18 to 57 K. Nevertheless, starting from the same coordination polyhedral symmetry and N_2O_6 environment, it is clear that the nature of the alkylated group and/or the positions of the $hfac^-$ anions (which can depend on the steric hindrance of the alkylated group) have a crucial importance in the value of the energy barrier. Because complex $[Dy(hfac)_3(\mathbf{L})]\cdot 0.5CH_2Cl_2$ crystallizes in the triclinic $P\bar{1}$ space group and considering an effective spin $^1/_2$ at low temperature, the orientation of the **g** tensor can be determined by measuring the magnetization of a single crystal in the three perpendicular planes (Figure S6). This oriented single-crystal measurement revealed a uniaxial magnetic anisotropy with a Landé factor of 19.6 (20 expected for a pure $M_J = \pm^{15}/_2$ ground state) with the orientation of the main magnetic axis along the most negatively charged direction of the surrounding coordination, i.e., perpendicular to the plane containing the nitrogen atoms (Figure 3a).

SA-CASSCF/SI-SO calculations were performed on $[Dy(hfac)_3(\mathbf{L})]$ to rationalize the observed magnetic properties (see the computational details in the SI). Energy spectra and **g** tensors for the eight Kramers doublets of the ground-state $^6H_{15/2}$ multiplet of the Dy^{III} ion are given in Table S5. The calculations

DOI: 10.1021/acs.inorgchem.8b02830
Inorg. Chem. 2019, 58, 52−56

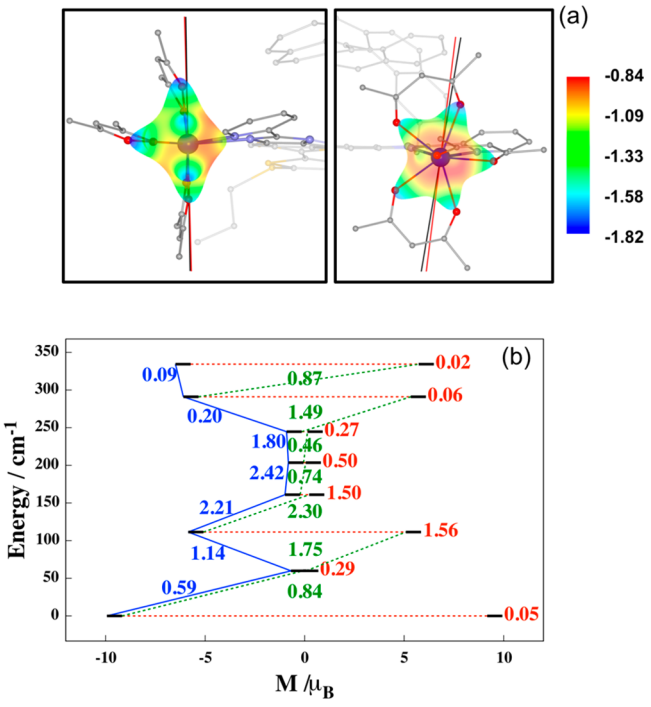

Figure 3. (a) Representation (two different orientations) of the ground-state total molecular electrostatic potential around the Dy^{III} ion. The black and red lines correspond to the experimental and theoretical main anisotropy axes, respectively. (b) Computed magnetization blocking barriers. The numbers provided for each line are the mean absolute values for the corresponding matrix elements of the magnetic transition dipole moment.

confirm the axial character of the magnetic anisotropy tensor of the ground-state Kramers doublet with a large g_z value of 19.09 for the Dy^{III} center and almost negligible g_x and g_y values. The decomposition in terms of pure $|J = {}^{15}/_{2}\rangle$ spin wave functions shows that the ground state has a majority (88%) $|\pm{}^{15}/_{2}\rangle$ character with a nonnegligible (10%) $|\pm{}^{11}/_{2}\rangle$ component with a first excited state lying at more than 75 K above the ground state. Such a discrepancy with the hypothetical energy barrier coming from an Orbach process (21.1 K) supports the only operative Raman relaxation process in $[Dy(hfac)_3(\mathbf{L})]\cdot 0.5CH_2Cl_2$. The calculated ground-state easy axis (Figure 3a) for the Dy^{III} ion is oriented perpendicular to the plane formed by the {tetrathiafulvalenyl-1*H*-benzimidazol-2-yl}pyridine moiety, in agreement with the experiment.[35]

This orientation is further supported by the representation of the molecular electrostatic potential around the Dy^{III} ion using the home-made *CAMMEL* program (*C*alculated *M*olecular *M*ultipolar *El*ectrostatics; the description of the code is detailed in the SI). The total electrostatic potential is represented for the ground state along with both the experimental and calculated axes in Figure 3a. As one can see, the most negative potential, containing the calculated magnetic axis, appears along the plane containing the two $hfac^-$ ligands and perpendicular to the TTF plane. Moreover, the multipolar expansion of the total molecular electrostatic potential (Figures S7−S9) shows that quadrupolar contributions seem to be preponderant, as was already observed in previous studies.[36,37] Regarding the static magnetic properties, this electronic structure leads to a calculated magnetization at 2 K in good agreement with the experimental *M* versus *H* and to a quantitative agreement with the thermal dependence of the $\chi_M T$ product (Figure 2), with some small discrepancy at low temperatures that may be due to possible intermolecular dipolar interactions. The computed magnetization blocking barrier is reported in Figure 3b. Even though the main relaxation mechanisms probably involve higher excited states (up to the third), calculations also support QTM within the ground-state doublet. However, these transition moments allow only a qualitative evaluation of the magnetization barrier because not all contributions (e.g., spin-phonon coupling) are included.[38−40]

In conclusion, a redox-active chiral-field-induced SMM, $[Dy(hfac)_3(\mathbf{L})]\cdot 0.5CH_2Cl_2$, has been successfully synthesized by the combination of a redox-active TTF-based skeleton and a [6]Helicene derivative, followed by the coordination reaction of the $Dy(hfac)_3$ precursor. This complex exhibits field-induced SMM behavior. This compound paves the way to redox modulation of the electronic circular dichroism signal and SMM behavior. To reach such a goal, the synthesis of pure enantiomers of $[Dy(hfac)_3(\mathbf{L})]\cdot 0.5CH_2Cl_2$ and the oxidation of **L** are in progress.

■ ASSOCIATED CONTENT

Supporting Information

The Supporting Information is available free of charge on the ACS Publications website at DOI: 10.1021/acs.inorgchem.8b02830.

ORTEP view of $[Dy(hfac)_3(\mathbf{L})]\cdot 0.5CH_2Cl_2$ (Figure S1), crystallographic data (Tables S1 and S2), cyclic voltamograms (Figure S2 and Table S3), additional magnetic data (Figures S4−S9 and Tables S4 and S5), experimental and material details, and computational details (PDF)

Accession Codes

CCDC 1867478 contains the supplementary crystallographic data for this paper. These data can be obtained free of charge via www.ccdc.cam.ac.uk/data_request/cif, or by emailing data_request@ccdc.cam.ac.uk, or by contacting The Cambridge Crystallographic Data Centre, 12 Union Road, Cambridge CB2 1EZ, UK; fax: +44 1223 336033.

■ AUTHOR INFORMATION

Corresponding Authors

*E-mail: fabrice.pointillart@univ-rennes1.fr.
*E-mail: jeanne.crassous@univ-rennes1.fr.
*E-mail: boris.leguennic@univ-rennes1.fr.

ORCID

Fabrice Pointillart: 0000-0001-7601-1927
Ludovic Favereau: 0000-0001-7847-2911
Federico Totti: 0000-0003-4752-0495
Jeanne Crassous: 0000-0002-4037-6067
Olivier Cador: 0000-0003-2064-6223
Boris Le Guennic: 0000-0003-3013-0546

Notes

The authors declare no competing financial interest.

■ ACKNOWLEDGMENTS

This work was supported by Région Bretagne, Rennes Métropole, CNRS, Université de Rennes 1, the ANR (Grant ANR-13-BS07-0022-01), and the ERC-CoG 725184 MULTIPROSMM (Project 725184). G.F.G. and V.M. gratefully acknowledge the European Commission through the ERC-AdG 267746 MolNanoMas (Project 267746) and ANR (Grant ANR-13-BS07-0022-01) for financial support. B.L.G., G.F.G.,

DOI: 10.1021/acs.inorgchem.8b02830
Inorg. Chem. 2019, 58, 52−56

and V.M. thank the French GENCI/IDRIS-CINES center for high-performance computing resources.

REFERENCES

(1) Guo, F.-S.; Day, B. M.; Chen, Y.-C.; Tong, M.-L.; Mansikkamäki, A.; Layfield, R. A. A Dysprosium Metallocene Single-Molecule Magnet Functioning at the Axial Limit. *Angew. Chem., Int. Ed.* **2017**, *56*, 11445−11449.

(2) Goodwin, C. A. P.; Ortu, F.; Reta, D.; Chilton, N. F.; Mills, D. P. Molecular magnetic hysteresis at 60 K in dysprosocenium. *Nature* **2017**, *548*, 439−442.

(3) Guo, F.-S.; Day, B. M.; Chen, Y.-C.; Tong, M.-L.; Mansikkamäki, A.; Layfield, R. A. Magnetic hysteresis up to 80 kelvin in a dysprosium metallocene single-molecule magnet. *Science* **2018**, eaav0652.

(4) Mannini, M.; Pineider, F.; Sainctavit, P.; Danieli, C.; Otero, E.; Sciancalepore, C.; Talarico, A.-M.; Arrio, M.-A.; Cornia, A.; Gatteschi, D.; Sessoli, R. Magnetic memory of a single-molecule quantum magnet wired to a gold surface. *Nat. Mater.* **2009**, *8*, 194−197.

(5) Pedersen, K. S.; Ariciu, A.; McAdams, S.; Weihe, H.; Bendix, J.; Tuna, F.; Piligkos, S. Toward Molecular 4f Single-Ion Magnet Qubits. *J. Am. Chem. Soc.* **2016**, *138*, 5801−5804.

(6) Rocha, A. R.; García-Suarez, V. M.; Bailey, S. W.; Lambert, C. J.; Ferrer, J.; Sanvito, S. Towards Molecular Spintronics. *Nat. Mater.* **2005**, *4*, 335−339.

(7) Pointillart, F.; Le Guennic, B.; Golhen, S.; Cador, O.; Ouahab, L. Slow magnetic relaxation in radical cation tetrathiafulvalene-based lanthanide(III) dinuclear complexes. *Chem. Commun.* **2013**, *49*, 11632−11634.

(8) Long, J.; Rouquette, J.; Thibaud, J.-M.; Ferreira, R. A. S.; Carlos, L. D.; Donnadieu, B.; Vieru, V.; Chibotaru, L. F.; Konczewicz, L.; Haines, J.; Guari, Y.; Larionova, J. A High-Temperature Molecular Ferroelectric Zn/Dy Complex Exhibiting Single-Ion-Magnet Behavior and Lanthanide Luminescence. *Angew. Chem., Int. Ed.* **2015**, *54*, 2236−2240.

(9) Liu, C. M.; Zhang, D.-Q.; Zhu, D.-B. Field-Induced Single-Ion Magnets Based on Enantiopure Chiral β-Diketonate Ligands. *Inorg. Chem.* **2013**, *52*, 8933−8940.

(10) Ou-Yang, J.-K.; Saleh, N.; Fernandez Garcia, G.; Norel, L.; Pointillart, F.; Guizouarn, T.; Cador, O.; Totti, F.; Ouahab, L.; Crassous, J.; Le Guennic, B. Improved slow magnetic relaxation in optically pure helicene-based Dy^{III} single molecule magnets. *Chem. Commun.* **2016**, *52*, 14474−14477.

(11) Fernandez-Garcia, G.; Flores Gonzalez, J.; Ou-Yang, J.-K.; Saleh, N.; Pointillart, F.; Cador, O.; Guizouarn, T.; Totti, F.; Ouahab, L.; Crassous, J.; Le Guennic, B. Slow Magnetic Relaxation in Chiral Helicene-Based Coordination Complex of Dysprosium. *Magnetochemistry* **2017**, *3*, 2−13.

(12) Shen, Y.; Chen, C.-F. *Helicenes Chemistry: From Synthesis to Applications*; Springer: Berlin, 2017.

(13) Shen, C.; Loas, G.; Srebro-Hooper, M.; Vanthuyne, N.; Toupet, L.; Cador, O.; Paul, F.; Lopez Navarrete, J. T.; Ramirez, F. J.; Nieto-Ortega, B.; Casado, J.; Autschbach, J.; Vallet, M.; Crassous, J. Iron Alkynyl Helicenes: Redox-Triggered Chiroptical Tuning in the IR and Near-IR Spectral Regions and Suitable for Telecommunications Applications. *Angew. Chem., Int. Ed.* **2016**, *55*, 8062−8066. Shen, C.; et al. Iron Alkynyl Helicenes: Redox-Triggered Chiroptical Tuning in the IR and Near-IR Spectral Regions and Suitable for Telecommunications Applications. *Angew. Chem.* **2016**, *128*, 8194−8198.

(14) Schweinfurth, D.; Zalibera, M.; Kathan, M.; Shen, C.; Mazzolini, M.; Trapp, N.; Crassous, J.; Gescheidt, G.; Diederich, F. Helicene Quinones: Redox-Triggered Chiroptical Switching and Chiral Recognition of the Semiquinone Radical Anion Lithium Salt by Electron Nuclear Double Resonance Spectroscopy. *J. Am. Chem. Soc.* **2014**, *136*, 13045−13052.

(15) Pospíšil, L.; Bednárová, L.; Štěpánek, P.; Slavíček, P.; Vávra, J.; Hromadová, M.; Dlouhá, H.; Tarábek, J.; Teplý, F. Intense Chiroptical Switching in a Dicationic Helicene-Like Derivative: Exploration of a Viologen-Type Redox Manifold of a Non-Racemic Hequat. *J. Am. Chem. Soc.* **2014**, *136*, 10826−10829.

(16) Biet, T.; Fihey, A.; Cauchy, T.; Vanthuyne, N.; Roussel, C.; Crassous, J.; Avarvari, N. Ethylenedithio-Tetrathiafulvalene-Helicenes: Electroactive Helical Precursors with Switchable Chiroptical Properties. *Chem. - Eur. J.* **2013**, *19*, 13160−13167.

(17) Kobayashi, H.; Kobayashi, A.; Cassoux, P. BETS as a source of molecular magnetic superconductors (BETS = bis(ethylenedithio)-tetraselenafulvalene. *Chem. Soc. Rev.* **2000**, *29*, 325−333.

(18) Coronado, E.; Galan-Mascaros, J. R.; Gomez-Garcia, C. J.; Laukhin, V. Coexistence of ferromagnetism and metallic conductivity in a molecule-based layered compound. *Nature* **2000**, *408*, 447−449.

(19) Zhang, G.; Zhang, D.; Guo, X.; Zhu, D. A new Redox-Fluorescence Switch Based on a Triad with Tetrathiafulvalene and Antracene Units. *Org. Lett.* **2004**, *6* (8), 1209−1212.

(20) Bendikov, M.; Wudl, F.; Perepichka, D. F. Tetrathiafulvalene, and their buckminsterfullerene derivatives: the brick and mortar of organic electronics. *Chem. Rev.* **2004**, *104*, 4891−4945.

(21) Lorcy, D.; Bellec, N.; Fourmigué, M.; Avarvari, N. Tetrathiafulvalene-based group XV ligands: synthesis, coordination chemistry and radical cation salts. *Coord. Chem. Rev.* **2009**, *253*, 1398−1438.

(22) Pointillart, F.; Le Guennic, B.; Cador, O.; Maury, O.; Ouahab, L. Lanthanide Ion and Tetrathiafulvalene-Based Ligand as a "magic" Couple toward Luminescence, Single-Molecule Magnets, and Magnetostructural Correlations. *Acc. Chem. Res.* **2015**, *48*, 2834−2842.

(23) Wu, J.; Dupont, N.; Liu, S.-X.; Neels, A.; Hauser, A.; Decurtins, S. Imidazole-Annulated Tetrathiafulvalene Exhibiting pH-Tuneable Intramolecular Charge Transfer and Redox Properties. *Chem. - Asian J.* **2009**, *4*, 392−399.

(24) Storch, J.; Zadny, J.; Strasak, T.; Kubala, M.; Sykora, J.; Dusek, M.; Cirkva, V.; Matejka, P.; Krbal, M.; Vacek, J. Synthesis and Characterization of a Helicene-Based Imidazolium Salt and Its Application in Organic Molecular Electronics. *Chem. - Eur. J.* **2015**, *21*, 2343−2347.

(25) Llunell, M.; Casanova, D.; Cirera, J.; Bofill, J. M.; Alemany, P.; Alvarez, S. S. *SHAPE*, version 2.1; Universitat de Barcelona: Barcelona, Spain, 2013.

(26) Cosquer, G.; Pointillart, F.; Golhen, S.; Cador, O.; Ouahab, L. Slow Magnetic relaxation in Condensed versus Dispersed Dysprosium-(III) Mononuclear Complexes. *Chem. - Eur. J.* **2013**, *19*, 7895−7903.

(27) Pointillart, F.; Guizouarn, T.; Lefeuvre, B.; Golhen, S.; Cador, O.; Ouahab, L. Rational Design of a Lanthanide-Based Complex Featuring Different Single-Molecule Magnets. *Chem. - Eur. J.* **2015**, *21*, 16929−16934.

(28) Speed, S.; Feng, M.; Fernandez Garcia, G.; Pointillart, F.; Lefeuvre, B.; Riobé, F.; Golhen, S.; Le Guennic, B.; Totti, F.; Guyot, Y.; Cador, O.; Maury, O.; Ouahab, L. Lanthanide complexes involving multichelating TTF-based ligands. *Inorg. Chem. Front.* **2017**, *4*, 604−617.

(29) Zadrozny, J. M.; Atanasov, M.; Bryan, A. M.; Lin, C.-Y.; Rekken, B. D.; Power, P. P.; Neese, F.; Long, J. R. Slow magnetization dynamics in a series of two-coordinate iron(II) complexes. *Chem. Sci.* **2013**, *4*, 125−138.

(30) Dekker, C.; Arts, A. F. M.; de Wijn, H. W.; van Duyneveldt, A. J.; Mydosh, J. A. Activated dynamics in a two-dimensional Ising spin glass: $Rb_2Cu_{1-x}Co_xF_4$. *Phys. Rev. B: Condens. Matter Mater. Phys.* **1989**, *40*, 11243−11251.

(31) Tang, J.; Zhang, P. *Lanthanide Single Molecule Magnets*; Springer-Verlag: Berlin, 2015.

(32) Goodwin, C. A. P.; Reta, D.; Ortu, F.; Chilton, N. F.; Mills, D. P. Synthesis and Electronic Structures of Heavy Lanthanide Metallocenium Cations. *J. Am. Chem. Soc.* **2017**, *139*, 18714−18724.

(33) Cole, K. S.; Cole, R. H. Dipersion and Absorption in Dielectrics I. Alternating Current Characteristics. *J. Chem. Phys.* **1941**, *9*, 341−351.

(34) Kishi, Y.; Cornet, L.; Pointillart, F.; Riobé, F.; Lefeuvre, B.; Cador, O.; Le Guennic, B.; Maury, O.; Fujiwara, H.; Ouahab, L. Luminescence and Single-Molecule Magnet Behaviour in Lanthanide Coordination Complexes Involving Benzothiazole-Based tetrathiafulvalene Ligands. *Eur. J. Inorg. Chem.* **2018**, 458.

DOI: 10.1021/acs.inorgchem.8b02830
Inorg. Chem. 2019, 58, 52−56

(35) da Cunha, T. T.; Jung, J.; Boulon, M. E.; Campo, G.; Pointillart, F.; Pereira, C. L. M.; Le Guennic, B.; Cador, O.; Bernot, K.; Pineider, F.; Golhen, S.; Ouahab, L. Magnetic Poles Determinations and Robustness of Memory Effect upon Solubilization in a Dy^{III}-Based Single Ion Magnet. *J. Am. Chem. Soc.* **2013**, *135*, 16332−16335.
(36) Zhang, K.; Montigaud, V.; Cador, O.; Li, G.-P.; Le Guennic, B.; Tang, J.; Wang, Y.-Y. Tuning Magnetic Interactions in Dy(III)4 Single-Molecule Magnets. *Inorg. Chem.* **2018**, *57*, 8550−8557.
(37) Huang, G.; Fernandez Garcia, G.; Badiane, I.; Camarra, M.; Freslon, S.; Guillou, O.; Daiguebonne, C.; Totti, F.; Cador, O.; Guizouarn, T.; Le Guennic, B.; Bernot, K. Magnetic slow relaxation in a Metal Organic Framework made of chains of ferromagnetically coupled Single-Molecule Magnets. *Chem. - Eur. J.* **2018**, *24*, 6983−6991.
(38) Escalera-Moreno, L.; Suaud, N.; Gaita-Arino, A.; Coronado, E. Determining Key Local Vibrations in the Relaxation of Molecular Spin Qubits and Single-Molecule Magnets. *J. Phys. Chem. Lett.* **2017**, *8*, 1695−1700.
(39) Lunghi, A.; Totti, F.; Sanvito, S.; Sessoli, R. Intra-molecular origin of the spin-phonon coupling in slow-relaxing molecular magnets. *Chem. Sci.* **2017**, *8*, 6051−6059.
(40) Lunghi, A.; Totti, F.; Sessoli, R.; Sanvito, S. The role of anharmonic phonons in under-barrier spin relaxation of single molecule magnets. *Nat. Commun.* **2017**, *8*, 14620−14626.

DOI: 10.1021/acs.inorgchem.8b02830
Inorg. Chem. 2019, 58, 52−56